J. Fluid Mech. (2002), *vol.* 468, *pp.* 271–281.
DOI: 10.1017/S0022112002001659 Printed in the United Kingdom

Numerical simulation of turbulent drag reduction using micro-bubbles

By JIN XU, MARTIN R. MAXEY AND GEORGE EM KARNIADAKIS

Division of Applied Mathematics, Brown University, Providence, RI 02912, USA

(Received 2 May 2002 and in revised form 5 June 2002)

While turbulent drag reduction through the injection of micro-bubbles into a turbulent boundary layer is well established in experiments, there is a lack of corresponding supporting evidence from direct numerical simulations. Here we report on a series of numerical simulations of small bubbles seeded in a turbulent channel flow at average volume fractions of up to 8%. These results show that even for relatively large bubbles, an initial transient drag reduction can occur as bubbles disperse into the flow. Relatively small spherical bubbles will produce a sustained level of drag reduction over time.

1. Introduction

Among the most successful and robust methods for drag reduction in a turbulent boundary layer has been the injection of gas micro-bubbles into the liquid flow. This phenomenon was first demonstrated by McCormick & Bhattacharyya (1973) and subsequentially verified in a series of experiments by Madavan, Deutsch & Merkle (1984, 1985); see also the review article of Merkle & Deutsch (1989). More recent experiments have been reported by Kato *et al.* (1995) and Guin, Kato & Takahashi (1998). In most of the experiments, gas is injected through a porous plate mounted on the wall of an open boundary layer flow or one side of a channel flow. The injection of the micro-bubbles leads to significant drag reduction, as measured by the frictional wall stress, over a significant distance downstream of the injection site. Reductions of 20–30% are readily achieved, and there is a nearly linear increase in the drag reduction, up to 50% or 60%, as the relative gas flow rate is increased.

So far there have not been any direct numerical simulations of micro-bubble drag reduction with the exception of some preliminary results by Kanai & Miyata (2001). They have reported numerical simulations of bubbly, turbulent channel flow where the flow is seeded with 27 bubbles of diameter 0.16 in a unit cube flow domain and average void fraction of 6%; however, their results are inconclusive.

Many factors contribute to the observed dynamics of micro-bubble drag reduction. These may include void fraction levels, bubble size, bubble deformation, bubble splitting or coalescence, buoyancy and correlations between the bubble motion and that of the turbulent fluctuations, not to mention the way in which the bubbles are injected into the flow. In this study we focus on a simpler, limited set of issues most relevant to the influence of the smaller bubbles. Specifically for small micro-bubbles, surface tension has a strong effect and the bubbles remain essentially spherical. This is characterized by the Weber number, which for a bubble of radius a in a turbulent channel flow may be defined in terms of the friction velocity scale u_* and fluid

density ρ as $We = \rho u_*^2 a/\gamma$, where γ is the coefficient of surface tension. The value of We is small for micro-bubbles under a range of operating conditions. Additionally, small bubbles in water, especially in seawater, tend rapidly to become coated with surface contaminants. As a result, it is often observed that a small bubble will respond approximately as a rigid body, see Magnaudet & Eames (2000); Clift, Grace & Weber (1978) and Detsch (1991). The effect of surfactants on bubble dynamics is still an open issue as illustrated by the recent work by Zhang, McLaughlin & Finch (2001).

In this paper we consider the effects of bubble seeding levels, bubble size and interactions with the turbulent flow. We present results of direct numerical simulations of a turbulent channel flow that is seeded with small, rigid, spherical bubbles up to an average void fraction of 8%. The monodisperse bubbles are initially distributed in layers near each wall and then disperse through the channel under the action of the turbulence. The drag force on each wall, corresponding changes in mean pressure gradient, and void fraction profiles are calculated. The results provide clear evidence of drag reduction produced by the smaller bubbles, based on these assumptions.

2. Channel flow simulations

2.1. *Equations of motion*

The presence of the bubbles and their influence on the flow is represented by the force-coupling method (FCM) introduced by Maxey *et al.* (1997) and developed by Maxey & Patel (2001) and Lomholt, Stenum & Maxey (2002). Each bubble is represented by a finite force monopole that generates a body force distribution $\boldsymbol{f}(\boldsymbol{x}, t)$, which transmits the resultant force of the bubbles on the flow to the fluid. The velocity field $\boldsymbol{u}(\boldsymbol{x}, t)$ is incompressible and satisfies

$$\rho \frac{\mathrm{D}\boldsymbol{u}}{\mathrm{D}t} = -\nabla p + \mu \nabla^2 \boldsymbol{u} + \boldsymbol{f}(\boldsymbol{x}, t), \tag{2.1}$$

$$\nabla \cdot \boldsymbol{u} = 0, \tag{2.2}$$

where μ is the fluid viscosity and p is the pressure. The body force due to the presence of N_B bubbles is

$$\boldsymbol{f}(\boldsymbol{x}, t) = \sum_{n=1}^{N_B} \boldsymbol{F}^{(n)} \Delta(\boldsymbol{x} - \boldsymbol{Y}^{(n)}(t)), \tag{2.3}$$

where $\boldsymbol{Y}^{(n)}$ is the position of the nth spherical bubble and $\boldsymbol{F}^{(n)}$ is the force this exerts on the fluid. The force monopole for each bubble is determined by the function $\Delta(\boldsymbol{x})$ which is specified as a Gaussian function

$$\Delta(\boldsymbol{x}) = (2\pi\sigma^2)^{-3/2} \exp(-\boldsymbol{x}^2/2\sigma^2) \tag{2.4}$$

and the length scale σ is set in terms of the bubble radius a as $a/\sigma = \sqrt{\pi}$. The velocity of each bubble $\boldsymbol{V}^{(n)}(t)$ is found by forming a local average of the fluid velocity over the region occupied by the bubble as

$$\boldsymbol{V}^{(n)}(t) = \int \boldsymbol{u}(\boldsymbol{x}, t) \Delta(\boldsymbol{x} - \boldsymbol{Y}^{(n)}(t)) \, \mathrm{d}^3\boldsymbol{x}. \tag{2.5}$$

The dynamics of the bubbles and the fluid are considered as one system where fluid drag on the bubbles, added-mass effects and lift forces are internal to the system. The equations of fluid motion are applied to the whole domain, including the volume nominally occupied by the bubbles. In this way the body forces induce a fluid motion

equivalent to that of the bubbles. If m_B and m_F denote the mass of a bubble and the mass of displaced fluid, the force of the bubble acting on the fluid is

$$\boldsymbol{F}^{(n)} = (m_B - m_F)\left(\boldsymbol{g} - \frac{\mathrm{d}\boldsymbol{V}^{(n)}}{\mathrm{d}t}\right), \tag{2.6}$$

where $\boldsymbol{g}$ is the acceleration due to gravity. This force is the sum of the net external force due to buoyancy of the bubble and the excess inertia of the bubble over the corresponding volume of displaced fluid. For the present study we exclude the effects of buoyancy and the mass of the bubble is neglected. In addition to the forces specified, a short-range conservative *force barrier* is imposed to represent collisions between bubbles and prevent overlap. A similar barrier force is imposed, normal to the wall, to represent collisions between a bubble and a rigid wall.

These equations can be solved analytically for conditions of Stokes flow, where they give good results for the motion of isolated particles, particle pairs and suspensions of particles at void fractions of less than 20% as shown by Maxey & Patel (2001). The results too are reliable for unsteady flow conditions, matching those obtained from particle-tracking equations such as in Maxey & Riley (1983). The results have been tested at finite particle Reynolds numbers, up to 40, by comparison with full direct numerical simulations, Dent (1999). Lomholt *et al.* (2002) provide comparisons with experiments at low to moderate Reynolds numbers for systems of 1 to 3 particles, again with good general agreement. The method does not resolve flow details near to the surface of a bubble or particle, and indeed the no-slip condition is not satisfied on the surface. Only the constraint (2.5) that the bubble moves with the velocity of the surrounding fluid is imposed. At distances of about half a particle radius from the surface the flow is well represented.

2.2. *Simulation procedures*

The wall boundaries of the channel flow are located at $x_2 = \pm h$ with the half-width of the channel $h = 1$. Periodic boundary conditions are applied in the streamwise and spanwise directions and the flow domain size $L_1 \times 2h \times L_3$ is $2\pi \times 2 \times 2\pi$. The velocity and pressure fields are represented by a Fourier expansion in x_1 and x_3, while in the wall-normal direction a spectral/*hp* element representation in terms of Jacobi polynomials is employed, Karniadakis & Sherwin (1999). The flow evolution is computed in terms of primitive variables using a high-order splitting scheme, Karniadakis & Sherwin (1999). In addition, a dealiasing procedure is applied in the Fourier expansion for the nonlinear terms, based on the standard 3/2-rule. In the present simulations the resolution employed for most runs is 64^3. Checks were also performed at a higher resolution of 96^3 and no significant differences in the flow statistics were found. A parallel version of the code was run using a domain decomposition technique. Typical runs even with 1600 bubbles increased the total cost by at most 10% compared to the cost of the single-phase runs.

The initial flow is taken from a DNS of a fully developed turbulent channel flow at a nominal Reynolds number of about 3000. The fluid velocity is scaled by the centreline velocity of a corresponding laminar Poiseuille flow so that the mean bulk velocity is 0.667. The volumetric flow rate through the channel is maintained at a constant value throughout the simulations and the mean pressure gradient then varies in response to fluctuations in the wall friction. Under these conditions the friction velocity Reynolds number $Re_* = u_* h/\nu = 135$. The bubbles are introduced into the flow in planar layers, parallel to the walls. The motion of the bubbles and the flow is

Simulation	Ia	Ib	Ic	II	III
a/h	0.1	0.1	0.1	0.15	0.3
$a^+ = au_*/\nu$	13.5	13.5	13.5	20	40.5
N_B	800	800	1600	242	60
Average void fraction (%)	4.24	4.24	8.5	4.3	8.6
Bubbles per layer	400	400	400	121	30
Layers near $x_2/h = -1$	1	2	2	1	1
Layers near $x_2/h = 1$	1	0	2	1	1
First layer position, y_0^+	20	20	20	25	50
Reduction in mean drag (%)	6.2	3.8	5.5	2.5	0.5

TABLE 1. Simulation parameters and drag reduction.

computed from the solution of the system of equations (2.1)–(2.5). Bubbles that exit the domain in the streamwise or spanwise directions are reintroduced into the flow to match the periodic boundary conditions.

3. Results

The simulations cover a range of bubble sizes, with radius $a/h = 0.1$, 0.15 or 0.3, and with average void fractions of 4% to 8%. We explore the effects of both bubble seeding of the flow and bubble size. The parameters for the different simulations and summary results are listed in table 1. In the first set of simulations (Ia–Ic) the effect of the initial seeding level was tested for the smaller bubbles. The bubbles were introduced in layers of 400 bubbles each, with the centres of the bubbles in the first layer at a distance $y_0^+ = 20$ from the wall. In simulations Ib and Ic a second layer was placed adjacent to the first, at a distance $y^+ = 54$ from the wall. The mean drag force is computed by integrating the mean viscous shear stress over each wall. The mean drag force averaged over the time interval $t = 10$–40, or $t^+ = 61$–243, is compared to the mean drag in the flow without bubbles and the results are listed in table 1. The results for simulations Ia and Ic both show a significant degree of drag reduction but the additional second layer, and the higher average void fraction, does not enhance the effect. Seeding bubbles near to just one wall, as in Ib, yields about half the overall level of drag reduction. There was no significant change in the mean wall stress on the opposite wall. Based on these results we focus attention on seeding the flow with a single layer adjacent to each wall.

The effects of different bubble size are seen by comparing the results of simulations Ia, II and III with the corresponding results for the flow without bubbles. We expect the larger bubbles to have a more limited response to the turbulence. First, there is the effect of spatial scale as the bubble velocity is influenced most by turbulent fluctuations on a scale larger than the bubble diameter. Second, the inertial response time of a bubble increases with bubble size, roughly as a^2. The integrated, viscous drag force on the two walls is shown in figure 1, where the results are normalized by the mean drag force in the flow without bubbles. For the two smaller sizes, Ia and II, the drag force shows a sustained reduction following an initial transient stage, with the bubbles of radius $a^+ = 13.5$ clearly being more effective for the same average void fraction. The larger bubbles (III) show a short-term decrease in the drag force before it increases to a larger than ambient level.

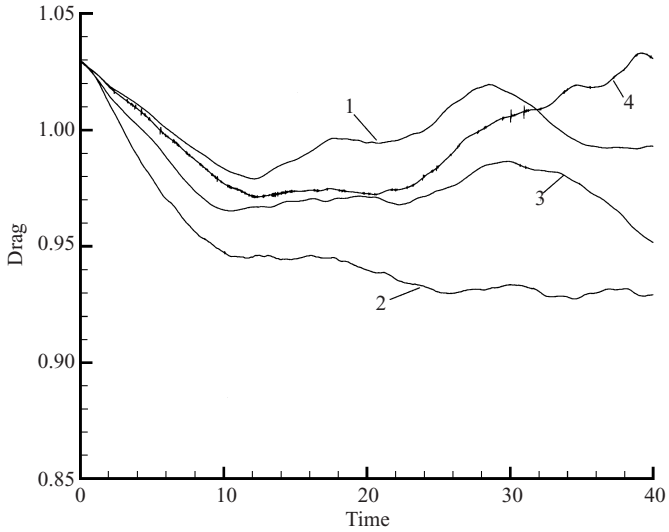

FIGURE 1. Normalized drag force versus time for different numbers and sizes of bubbles: (1) No bubbles; (2) (Ia); (3) (II); (4) (III).

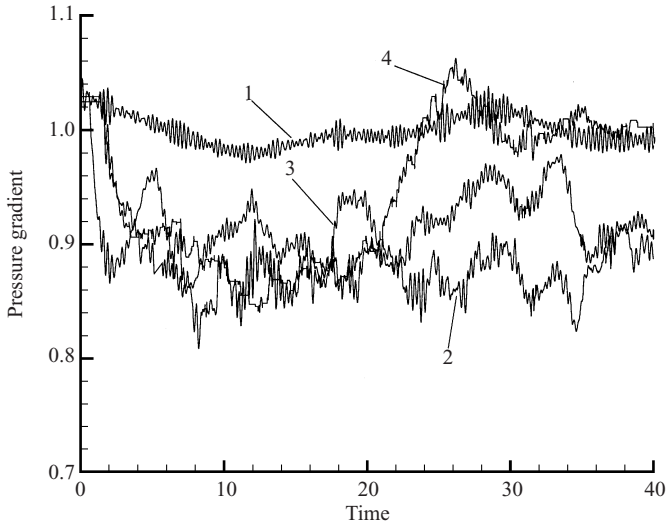

FIGURE 2. Normalized pressure drop versus time for different sized bubbles: (1) No bubbles; (2) (Ia); (3) (II); (4) (III).

Further information is provided by considering the time variations of the mean pressure gradient, shown in figure 2, for the bubbles of different size. While the mean pressure gradient in the turbulent flow without bubbles fluctuates in time, it remains stationary. The average value for the smallest bubbles, after an initial transient, is about 12–15% lower. The mean pressure gradient for the largest bubbles (III) is reduced for an interval before returning to the ambient level, or higher. In two-phase flow the mean pressure gradient is influenced by two factors. One is the mean viscous drag force on each wall, while the other is the acceleration of the bubble phase. The

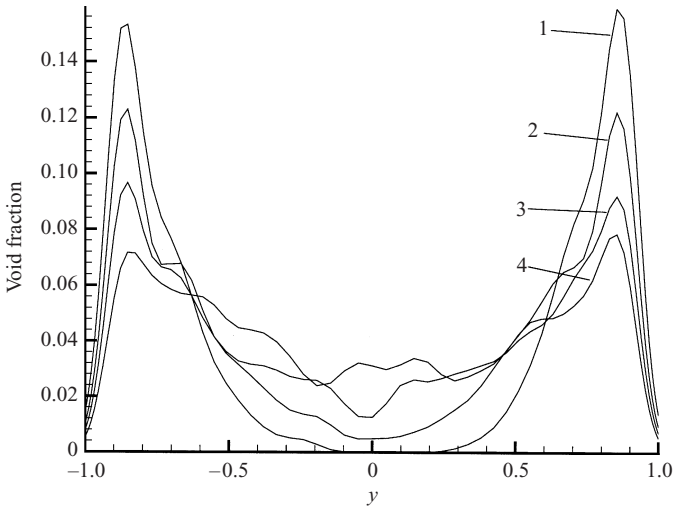

FIGURE 3. Concentration profiles across the channel for case (Ia): (1) $t = 10$; (2) $t = 20$; (3) $t = 30$; (4) $t = 40$.

total volume-integrated flow rate in the channel

$$\int_0^L \int_{-h}^h \int_0^L u_1 \, \mathrm{d}^3\boldsymbol{x} = Q_0 \tag{3.1}$$

is held constant throughout the simulation, $Q_0 = 16\pi^2/3$. The volume-integrated flow rate associated with the bubble phase is

$$\sum_{n=1}^{N_B} \Omega_B V_1^{(n)} = Q_B, \tag{3.2}$$

where Ω_B is the volume of one bubble and ρQ_B is the momentum deficit in the flow domain due to the presence of the bubbles. The corresponding flow rate for the liquid phase Q_L is $(Q_0 - Q_B)$. As the bubbles disperse from their initial locations, under the action of the turbulent flow, they migrate from the relatively slow flow regions near the walls to the faster flow in the core of the channel. This produces an increase in Q_B at least for some initial period. A control-volume integral of (2.1) for the flow domain $(L \times 2h \times L)$ gives the balance for the mean pressure gradient

$$-2hL^2 \frac{\mathrm{d}P}{\mathrm{d}x_1} = L^2\{\tau(-h) + \tau(h)\} - \rho \frac{\mathrm{d}Q_B}{\mathrm{d}t}, \tag{3.3}$$

where $\tau(-h)$, $\tau(h)$ are the mean viscous shear stresses at each wall, averaged over the plane of the wall. The pressure gradient required to sustain the flow is lower if either the mean drag is reduced or the bubble phase is accelerating.

In figure 3, mean void fraction profiles for the small bubbles (Ia) are given for different times. There are strong peaks of bubble concentration near each wall that reflect the initial seeding. These steadily decrease as the bubbles disperse across the channel, tending to a more uniform average distribution. The larger bubbles, (II) $a^+ = 20$, show very similar trends. For both, there is still a noticeably higher void fraction nearer to each wall even at the last time instant, $t = 40$. The value of Q_B increases steadily over this time interval and through the force balance (3.3) contributes to the reduction in the mean pressure gradient.

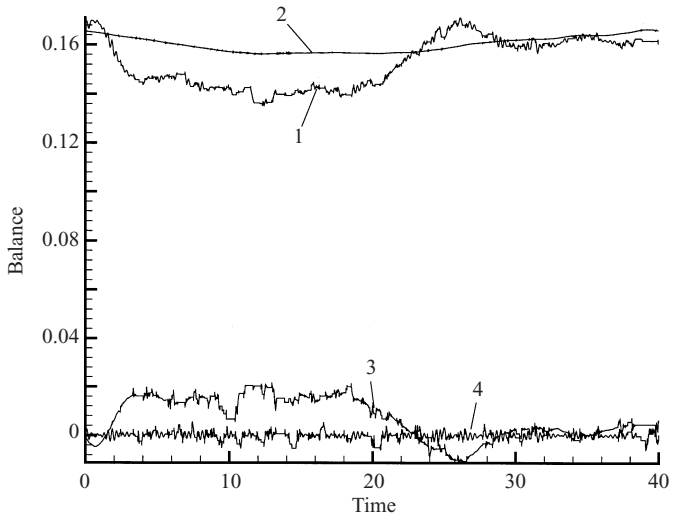

FIGURE 4. Time history of various terms in momentum balance for case (III): (1) pressure drop; (2) wall stress; (3) bubble acceleration; (4) residual.

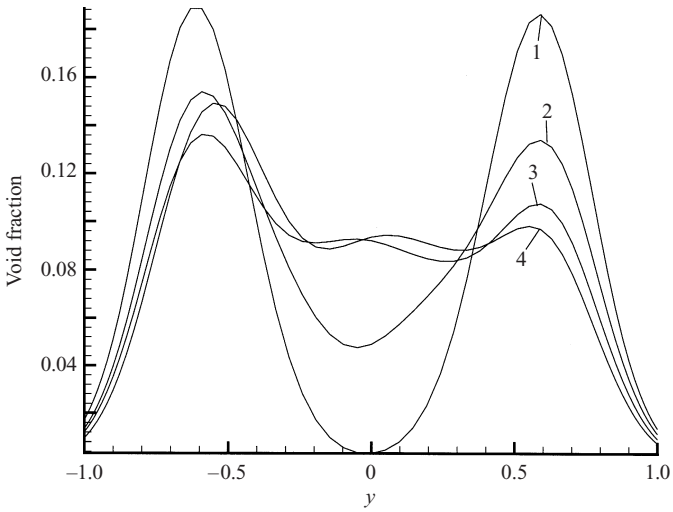

FIGURE 5. Concentration profiles across the channel for case (III): (1) $t = 10$; (2) $t = 20$; (3) $t = 30$; (4) $t = 40$.

The largest bubbles, (III) $a^+ = 41$, show a somewhat different trend. Figure 4 shows the various components of the force balance (3.3). Initially, the pressure gradient decreases in response to the net acceleration of the bubble phase, $\mathrm{d}Q_B/\mathrm{d}t > 0$. As shown in figure 1 there is a reduction in the drag force over the same period. Over the second half of the simulation, Q_B decreases while the pressure gradient increases and so too does the drag force. During this latter stage the bubble phase decelerates. In figure 5 the corresponding void fraction profiles are plotted. The profiles for the first three time instants show that the peak void fraction steadily decreases while over the last time interval, $t = 30$–40, the void fraction at $x_2 = -0.5$ increases as the void fraction at $x_2 = 0.5$ continues to decrease slowly. Here the bubbles that were initially

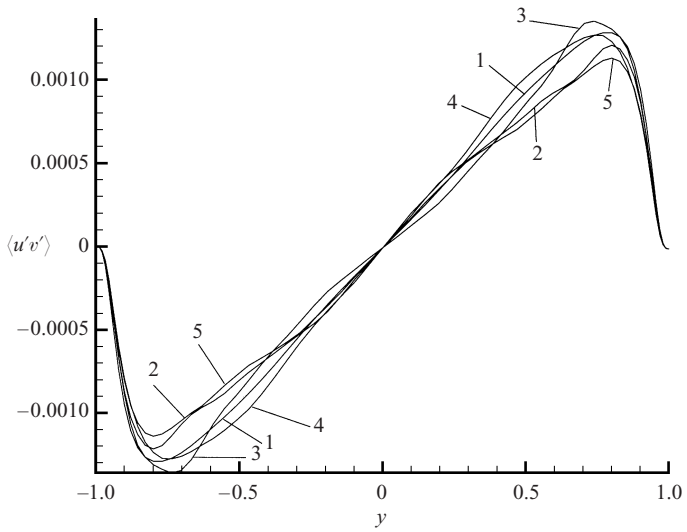

FIGURE 6. Reynolds stress profiles averaged over different intervals for case (Ia): (1) No bubbles; (2) $t = 0$–10; (3) $t = 10$–20; (4) $t = 20$–30; (5) $t = 30$–40.

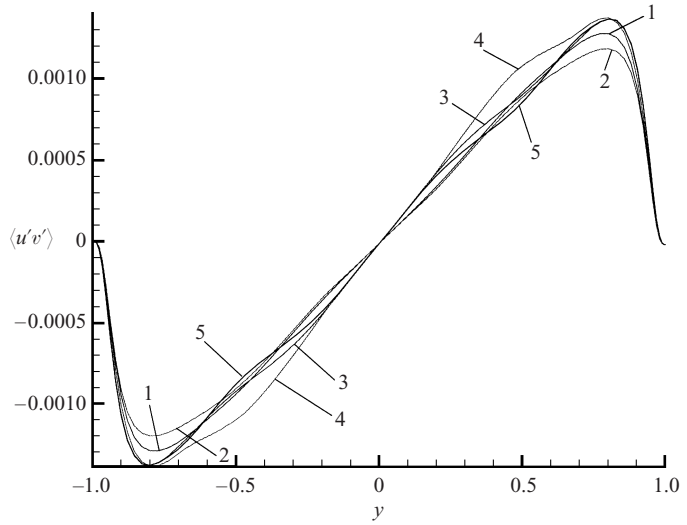

FIGURE 7. Reynolds stress profiles averaged over different intervals for case (III): (1) No bubbles; (2) $t = 0$–10; (3) $t = 10$–20; (4) $t = 20$–30; (5) $t = 30$–40.

in the upper half of the channel have crossed the centreline and are accumulating near the lower wall.

The results so far indicate that the initial seeding of the bubbles in the flow has an important effect on the pressure gradient and viscous drag force. The large bubbles give a *transient reduction* in drag while the smaller bubbles give a *sustained reduction* in drag. A further indication of how the flow is modified by the bubble phase is provided by the profiles of the unconditional Reynolds shear stress, computed from the flow field $\boldsymbol{u}(\boldsymbol{x}, t)$. These are plotted in figures 6 and 7 for bubbles of radius $a^+ = 13.5$ (Ia) and $a^+ = 41$(III) respectively. The Reynolds stresses, averaged over the four time intervals, for (Ia) are in general lower than the corresponding stresses for the

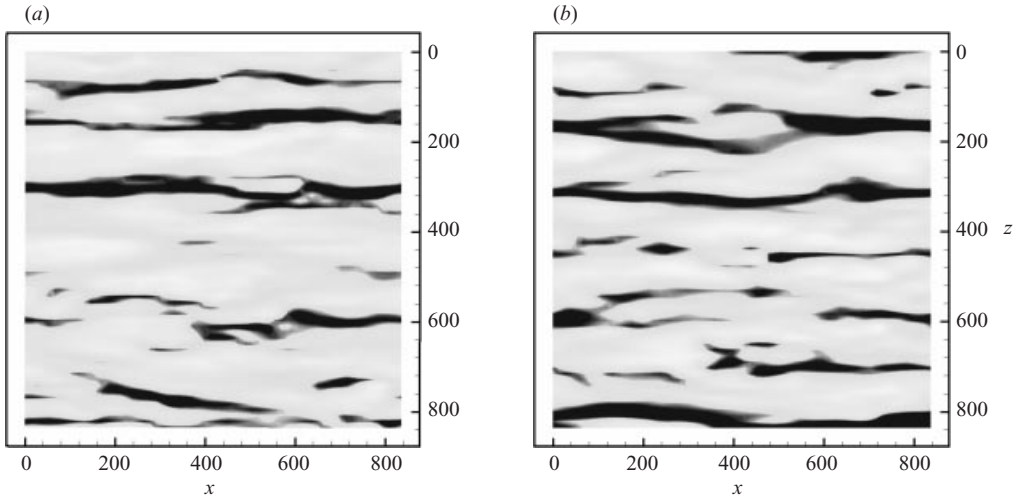

FIGURE 8. Contours of instantaneous streamwise velocity at $y^+ = 10$ visualizing the streaks: (*a*) case (Ia); (*b*) no bubbles.

turbulence without bubbles. In contrast the Reynolds stresses for the larger bubbles (III) are in general higher than the single-phase turbulence. The only exception is during the first time interval $t = 0$–10 when some drag reduction was observed in figure 2.

4. Discussion

The results presented give a clear indication of the reduction in drag force that can come from seeding a turbulent shear flow with micro-bubbles. The strongest, sustained reduction in drag is achieved for the small bubbles, $a^+ = 13.5$, and for these the assumption of spherical shape is the most reasonable. The results for the larger bubbles point to the limited response of these bubbles to the turbulence due to their increased size and time scales. They also illustrate the importance of the evolving void fraction distributions and the initial bubble seeding. As the bubbles disperse away from the walls and as the bubble flow rate Q_B increases, there is a displacement of liquid towards the walls from the centre region of the channel. An additional simulation was performed with the smaller bubbles, $a^+ = 13.5$, with 800 bubbles initially seeded uniformly at random in the flow and not concentrated in an initial layer near the wall. This flow eventually gave the same levels of reduced drag force as shown in figure 1, but in the initial transient stage there was only a small reduction in drag. These results point to at least three mechanisms involved: one linked to the initial seeding of the bubbles, the second associated with density effects, where the bubbles reduce the turbulent momentum transfer, and the third governed by specific correlations between the bubbles and the turbulence.

With regard to the modification of turbulent structures in the near-wall region we observe a very different picture than for other turbulent drag reduction techniques, e.g. riblets, travelling waves or polymers, see Du & Karnidakis (2000). Typically, when drag is reduced there is a modification of the sublayer and lifted streaks, which in most cases become more coherent while the spacing of the streaks increases. However, the instantaneous views of the streamwise velocity contours, shown in figure 8 at $y^+ = 10$,

do not have this feature as we compare data from the flow without bubbles to data from (Ia). The streaks seem to be affected very little for the cases we investigated here and they become slightly more disorderly due to the chaotic forcing imposed by the bubbles. In some relatively rare cases we observed that bubbles would tend to move towards the low-pressure regions, i.e. in the vicinity of low-speed streaks, but this was not a sustained feature. The Reynolds number for the present simulations is low and the viscous stresses of the mean flow are still important throughout the flow. This will limit the degree of drag reduction that can be achieved under these conditions. We are currently pursuing simulations at higher Reynolds numbers and with smaller bubbles to obtain a clearer characterization of the flow dynamics and the physical mechanisms involved. We will report such results in a future publication.

This work was supported by Defense Advanced Research Projects Agency, Advanced Technology Office, under the Friction Drag Reduction Program (ARPA order K042/07/39) contract number MDA972-01-C-0024. We would like to thank Sarah Dance and Steven Dong of Brown University and Professor Gretar Tryggvason of Worcester Polytechnic Institute for useful discussions. The computations were performed at the NCSA University of Illinois (Urbana-Champaign) and at the Center for Scientific Computing & Visualization at Brown University.

REFERENCES

Clift, R., Grace, J. & Weber, M. 1978 *Bubbles, Drops and Particles*. Academic.

Dent, G. 1999 Aspects of particle sedimentation in dilute flows at finite Reynolds numbers. PhD thesis, Brown University.

Detsch, R. 1991 Small air bubbles in reagent grade water and seawater: I. Rise velocities of 20 to 1000 μm diameter bubbles. *J. Geophys. Res.* **96**, 8901–8906.

Du, Y. & Karnidakis, G. 2000 Supressing wall turbulence by means of a transverse travelling wave. *Science* **288**, 1230–1234.

Guin, M., Kato, H. & Takahashi, Y. 1998 Experimental evidence for a link between microbubble drag reduction phenomena and periodically excited wall-bounded turbulent flow. In *Proc. Intl Symp. on Seawater Drag Reduction, Newport RI*, pp. 313–318. Newport, RI: Naval Undersea Warfare Center, c 1999.

Kanai, A. & Miyata, H. 2001 Direct numerical simulation of wall turbulent flows with microbubbles. *Intl J. Numer. Meth. Fluids* **35**, 593–615.

Karniadakis, G. & Sherwin, S. 1999 *Spectral/hp Element Methods for CFD*. Oxford University Press.

Kato, H., Miyanaga, M., Yamaguchi, H. & Guin, M. 1995 Frictional drag reduction by injecting bubbly water into turbulent boundary layer and the effect of plate orientation. In *Advances in Multiphase Flow* (ed. A. Serizawa, T. Fukano & J. Bataille), pp. 85–96. Elsevier.

Lomholt, S., Stenum, B. & Maxey, M. 2002 Experimental verification of the force coupling method for particulate flows. *Intl J. Multiphase Flow* **28**, 225–246.

Madavan, N., Deutsch, S. & Merkle, C. 1984 Reduction of turbulent skin friction by microbubbles. *Phys. Fluids* **27**, 356–363.

Madavan, N., Deutsch, S. & Merkle, C. 1985 Measurements of local skin friction in a microbubble-modified turbulent boundary layer. *J. Fluid Mech.* **156**, 237–256.

Magnaudet, J. & Eames, I. 2000 The motion of high Reynolds number bubbles in inhomogeneous flows. *Annu. Rev. Fluid Mech.* **32**, 659–708.

Maxey, M. & Patel, B. 2001 Localized force representations for particles sedimenting in Stokes flow. *Intl J. Multiphase Flow* **27**, 1603–1626.

Maxey, M., Patel, B., Chang, E. & Wang, L.-P. 1997 Simulations of dispersed turbulent multiphase flow. *Fluid Dyn. Res.* **32**, 143–156.

Maxey, M. & Riley, J. 1983 Equation of motion for a small rigid sphere in a non-uniform flow. *Phys. Fluids* **26**, 883–889.

McCormick, M. & Bhattacharyya, R. 1973 Drag reduction of a submersible hull by electrolysis. *Nav. Engng J.* **85**, 11.

Merkle, C. & Deutsch, S. 1989 Microbubble drag reduction. *Frontiers in Experimental Fluid Mechanics.* (ed. M. Gad-el-Hak) Lecture Notes in Engineering, vol. 46, p. 291. Springer

Zhang, Y., McLaughlin, J. & Finch, J. 2001 Bubble velocity profile and model of surfactant mass transfer to bubble surface. *Chem. Engng Sci.* **56**, 6605–6616.